THE JOURNAL OF BIOLOGICAL CHEMISTRY VOL. 286, NO. 34, pp. 30190–30199, August 26, 2011

Distinct Functional Domains Contribute to Degradation of the Low Density Lipoprotein Receptor (LDLR) by the E3 Ubiquitin Ligase Inducible Degrader of the LDLR (IDOL)

Received for publication, April 9, 2011, and in revised form, July 5, 2011 Published, JBC Papers in Press, July 6, 2011, DOI 10.1074/jbc.M111.249557

Vincenzo Sorrentino[‡], Lilith Scheer[‡], Ana Santos[‡], Eric Reits[§], Boris Bleijlevens[‡], and Noam Zelcer[‡1]

From the Departments of [‡]Medical Biochemistry and [§]Cell Biology and Histology, Academic Medical Center, University of Amsterdam, Meibergdreef 15, 1105 AZ Amsterdam, The Netherlands

We recently identified the liver X receptor-regulated E3 ubiquitin ligase inducible degrader of the LDL receptor (IDOL) as a modulator of lipoprotein metabolism. Acting as an E3 ubiquitin ligase, IDOL triggers ubiquitination and subsequent degradation of the low density lipoprotein receptor (LDLR). We demonstrate here that this outcome requires the conserved FERM and RING domains present in IDOL. The RING domain promotes ubiquitination *in vitro* and Lys-63-specific ubiquitination of the LDLR *in vivo* in response to IDOL or liver X receptor activation. We further identify RING residues that differentially influence ubiquitination of the LDLR or stability of IDOL. The FERM domain interacts with the LDLR and in living cells co-localizes with the receptor at the plasma membrane. Homology modeling revealed a phosphotyrosine-binding element embedded in the FERM domain. Mutating residues within this region or residues in the LDLR preceding the NPVY endocytosis motif abrogate LDLR degradation by IDOL. Collectively, our results indicate that both the FERM and RING domains are required for promoting lysosomal degradation of the LDLR by IDOL. Our findings may facilitate development of structure-based IDOL inhibitors aimed at increasing LDLR abundance in therapeutic strategies to treat cardiovascular disease.

Elevated levels of plasma low density lipoprotein (LDL) cholesterol represent a major risk factor for development of atherosclerosis (1). Because of its ability to mediate LDL uptake into cells, the LDL receptor (LDLR)[2] is an important determinant of plasma LDL levels and is a target for human cardiovascular therapy (2, 3). Mutations in this receptor are the leading cause of familial hypercholesterolemia, a disease characterized by reduced hepatic LDL clearance, elevated plasma cholesterol levels, and accelerated cardiovascular disease (3, 4). In line with the central role of the LDLR in LDL metabolism, its abundance is subject to tight regulation. Transcription of the *LDLR* is controlled by the sterol regulatory element-binding protein (SREBP) family of transcription factors and is increased when cellular cholesterol levels decline to allow efficient uptake of LDL-derived cholesterol (5). In addition to transcriptional regulation, the importance of post-transcriptional modulation of LDLR abundance has become apparent in recent years. Genetic studies identified mutations in the LDLR adaptor protein 1 (LDLRAP1/ARH) (6) and the SREBP target gene proprotein convertase subtilisin/kexin 9 (*PCSK9*) (7–9) that result in altered endocytosis, trafficking, and stability of the LDLR.

We have recently identified the E3 ubiquitin ligase inducible degrader of the LDLR (IDOL, also known as MYLIP (10)) as a post-transcriptional regulator of LDLR abundance (11). Unlike the *LDLR* and *Pcsk9*, *IDOL* is not regulated by SREBP. Rather, IDOL is a direct transcriptional target of the nuclear receptors liver X receptors (LXR) (*NR1H2* and *NR1H3*) and is induced by these transcription factors when cellular cholesterol levels rise (11, 12). As such, the LXR-IDOL-LDLR axis defines a complementary but distinct pathway for sterol-dependent control of cellular cholesterol uptake through the LDLR. We recently reported that in addition to the LDLR, two other closely related receptors, the VLDLR and APOER2, are also subject to IDOL-mediated degradation (13). Briefly, overexpression of IDOL strongly reduces LDLR, VLDLR, and APOER2 protein levels *in vitro* and *in vivo,* whereas IDOL knockdown results in the opposite outcome. Functionally, this is mirrored by altered LDL uptake in the case of the LDLR, or disturbed Reelin signaling in the case of the VLDLR or APOER2 (11, 13). Importantly, modulation of the levels of these receptors by IDOL is a post-transcriptional event. Ubiquitination of these receptors by IDOL marks them for subsequent lysosomal degradation.

Although our previous work demonstrates that IDOL decreases abundance of LDLR family members, the functional domains within IDOL that mediate this outcome have not yet been defined. In this study, we use a combination of assays to characterize the contribution of the N-terminal FERM and C-terminal RING domains to IDOL-mediated degradation of the LDLR and related receptors. These studies provide the first structural-functional characterization of the IDOL-LDLR interaction network.

EXPERIMENTAL PROCEDURES

Cell Culture and Transfections—HEK 293T and HepG2 cells were from the ATCC. Cells were maintained in DMEM (Invitrogen) supplemented with 10% FBS at 37 °C and 5% CO_2. HEK 293T and HepG2 cells were transfected with X-tremeGENE HP

[1] Supported by a career development award from the Human Frontier Science Program Organization and by a VIDI grant from the Netherlands Organization for Scientific Research. To whom correspondence should be addressed: Meibergdreef 15, 1105 AZ Amsterdam, The Netherlands. Tel.: 31-20-5665131; Fax: 31-20-6915519; E-mail: n.zelcer@amc.uva.nl.

[2] The abbreviations used are: LDLR, low density lipoprotein receptor; IDOL, inducible degrader of the LDLR; LXR, liver X receptor; PTB, phosphotyrosine binding domain; SREBP, sterol regulatory element-binding protein; BisTris, 2-[bis(2-hydroxyethyl)amino]-2-(hydroxymethyl)propane-1,3-diol; PDB, Protein Data Bank; VLDLR, VLDL receptor.

(Roche Applied Science) according to the manufacturer's instructions. The amount of IDOL, LDLR, and VLDLR expression plasmids used in these experiments is indicated in the figure legends. Transfection efficiency was monitored by transfection of an expression plasmid for GFP and was consistently >90% in HEK 293T cells.

Plasmids and Expression Constructs—Expression plasmids for IDOL, VLDLR, and LDLR were reported previously. The LDLR-HA and LDLR-Myc-His expression constructs were a gift from Dr. Trond Paul Leren (University of Oslo, Norway). The different IDOL deletion and domain expression plasmids were generated with gateway-mediated recombination (Invitrogen). The QuikChange site-directed mutagenesis kit (Stratagene) was used to introduce mutations in the LDLR and hIDOL. DNA sequencing was used to verify the correctness of all the constructs used in this study.

Antibodies, Immunoblot Analysis, and Immunoprecipitation—Total cell lysates were prepared in RIPA buffer (150 mM NaCl, 1% Nonidet P-40, 0.1% sodium deoxycholate, 0.1% SDS, 100 mM Tris-HCl, pH 7.4) supplemented with protease inhibitors (Roche Applied Science). Lysates were cleared by centrifugation at 4 °C for 10 min at 10,000 × *g*. Protein concentration was determined using the Bradford assay (Bio-Rad) with BSA as reference. Samples (10–40 μg) were separated on NuPAGE BisTris gels (Invitrogen) and transferred to nitrocellulose. Membranes were probed with the following antibodies: LDLR (Cayman Chemical, catalog no. 10007665, 1:2000), tubulin (Calbiochem, clone CP06, 1:10,000), HA (Covance, clone HA.11, 1:20,000), V5-HRP (Invitrogen, catalog no. R961, 1:5000), VLDLR (Santa Cruz Biotechnology, clone 6A6, 1:250), or α74 (1:20,000) (13), FLAG-HRP (Sigma, clone M2, 1:5000), ubiquitin (Biomol, clone FK2, 1:1000), and His_6 (1:2000, catalog no. 600-401-382, Rockland). IDOL was detected with polyclonal antibodies raised in rabbits (11). Secondary HRP-conjugated antibodies (Zymed Laboratories Inc.) were used and visualized with chemiluminescence on a Fuji LAS4000 (GE Healthcare). HA-tagged proteins were immunoprecipitated as described previously (11). All immunoblots are representative of at least two independent experiments.

Purification of Recombinant IDOL RING Domain Expressed in Escherichia coli—His_6-tagged hIDOL RING protein was produced in the bacterial RIPL strain (Novagen). Bacteria were grown in LB at 37 °C to an A_{600} of 0.6 and induced with 1 mM isopropyl 1-thio-β-D-galactopyranoside for 4 h. Bacterial pellets were collected and lysed in lysis buffer (50 mM Tris-HCl, pH 7.6, 0.5 M NaCl, 5 mM imidazole, and 1 mM DTT) supplemented with protease inhibitors and then sonicated on ice until cells were broken. Debris was removed by centrifugation, and the lysates were loaded onto HisTrap HP columns (GE Healthcare) coupled to an ÄKTAprime Plus protein purification system (GE Healthcare). Bound proteins were eluted with imidazole, buffer exchanged using Hi-Trap desalting columns (GE Healthcare), and collected in elution buffer (20 mM Tris-HCl, pH 7.6, 100 mM NaCl, 1 mM DTT). Aliquots were immediately frozen in liquid N_2 and stored at −80 °C.

In Vitro Ubiquitination Assay—Recombinant rabbit E1, UBCH5a, UBC13, and UEV1a were the kind gifts from Dr. Ben Distel (University of Amsterdam Medical Center, The Netherlands). Briefly, reactions were carried out at 28 °C for 2 h in 20-μl reactions containing 25 mM Tris, pH 8, 100 mM NaCl, 5 mM $MgCl_2$, 1 mM DTT, and some of the following: 5 mM ATP, 0.4 μg of recombinant rabbit E1, 0.4 μg of UBCH5a, 2.5 μg of ubiquitin (Biomol), and 0.4 μg of IDOL RING. In experiments with UBC13 and UEV1a, the mixtures were incubated at 37 °C for 3 h. Reactions were stopped by addition of SDS-PAGE loading buffer and subjected to immunoblotting as described above.

Molecular Modeling—Homology modeling of IDOL was performed using the ModWeb server for protein modeling. The protein sequence of the full-length IDOL was submitted as input for structure prediction. Calculated models were evaluated, and a structural prediction for IDOL residues 1–276 modeled on the FERM domain of protein 4.1 residues (1–279) was selected (PDB 1gg3) (14). Bioinformatic analysis revealed the presence of a partial PTB domain within this region of the IDOL protein, also identified in the predicted structure. The IDOL PTB domain was aligned to the DAB1 PTB domain binding the ApoER2 tail (PDB 1NTV) (15) allowing prediction of IDOL residues involved in substrate binding.

Live Confocal Imaging of Live Cells—HepG2 cells were plated on glass coverslips, transfected with LDLR-GFP, IDOL FERM-DsRed2 (IDOL residues 1–344), or a combination of both at a 1:1 ratio and cultured for 48 h. Confocal analysis was performed using a Leica TCS SP2 confocal system equipped with an Ar/Kr laser with a ×63 objective and a heated stage for living cell analysis at 37 °C.

RNA Isolation and Quantitative PCR—Total RNA was isolated from cells using TRIzol (Invitrogen). One microgram of total RNA was reverse-transcribed with random hexamers using iScript reverse transcription reagents kit (Bio-Rad). SYBR Green real time quantitative PCR assays were performed on a Lightcycler 480 II apparatus (Roche Applied Science). Results show averages of duplicate experiments normalized to 36B4. Primer sequences are available upon request.

RESULTS

The ability of the E3 ubiquitin ligase IDOL to post-transcriptionally modulate the abundance of several members of the LDLR family of receptors suggests it contains functional domains that promote substrate recognition and subsequent ubiquitination. IDOL consists of an N-terminal FERM domain and a C-terminal RING domain (Fig. 1*A*). To assess the contribution of these IDOL domains to degradation of the LDLR, we used a co-transfection assay in HEK 293T cells. In this assay, expression of wild type IDOL dramatically decreases abundance of the LDLR (Fig. 1*B*). As we have shown previously (11), mutation of a conserved cysteine residue (C387A; MUT) prevents IDOL from degrading the LDLR and substantially increases the stability of IDOL. Under these experimental conditions, we are also able to detect slower migrating IDOL bands that likely represent ubiquitinated IDOL (11). Independent expression of either the FERM or RING domains did not influence LDLR abundance (Fig. 1*B*), suggesting that both are required for IDOL to degrade the LDLR. To further map the IDOL regions required for degrading the LDLR, we generated incremental N-terminal deletions of predicted FERM subdomains. Despite similar transfection efficiencies, these con-

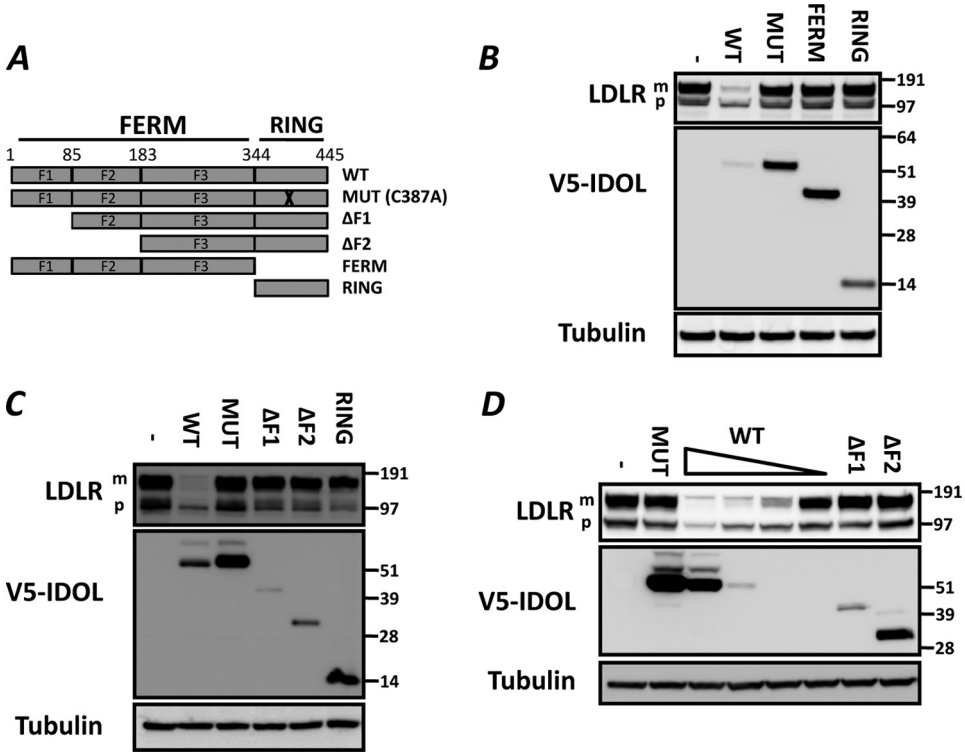

FIGURE 1. **Intact full-length IDOL is required for degrading the LDLR.** *A,* schematic representation of the IDOL protein. Depicted are the N-terminal FERM domain (1–344) and the C-terminal RING domain (344–445). *F1, F2,* and *F3* correspond to established FERM subdomain boundaries. *B–D,* HEK 293T cells were co-transfected with LDLR (100 ng) and V5-tagged IDOL domain (900 ng) expression plasmids. The V5-IDOL constructs correspond to those indicated in *A*. Total cell lysates were analyzed by immunoblotting as indicated. To titrate the level of wild type V5-IDOL in *D*, cells were transfected with 900, 150, 30, and 5 ng of the corresponding expression plasmid while maintaining an equal amount of total DNA in the transfection reactions. *MUT*, catalytically nonactive IDOL carrying the C387A mutation in the RING domain. The precursor (*p*) and mature (*m*) forms of the LDLR are indicated. Blots are representative of at least two independent experiments.

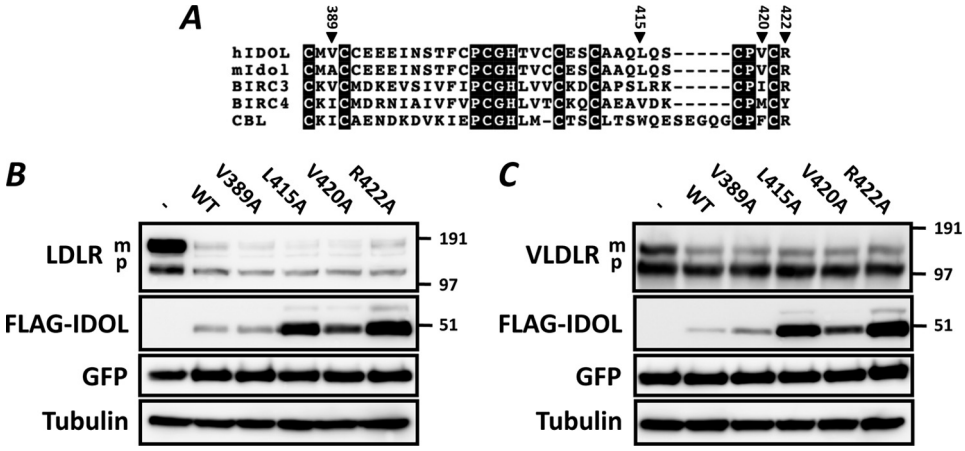

FIGURE 2. **Active IDOL RING domain is required for ubiquitination and degradation of the LDLR.** *A,* sequence homology of hIDOL (NP_037394), mIDOL (NP_722484), BIRC3 (NP_001156), BIRC4 (NP_001158), and CBL (NP_005179) RING domains. *Numbering* corresponds to residue number in hIDOL. *Closed triangles* indicate residues that were mutated in this study. *B* and *C,* HEK 293T cells were co-transfected with LDLR (800 ng) (*B*) or VLDLR (800 ng) (*C*), the indicated IDOL mutant (150 ng), and GFP (50 ng) expression plasmids. Total cell lysates were analyzed by immunoblotting as indicated. The precursor (*p*) and mature (*m*) forms of the LDLR are indicated. Blots are representative of at least two independent experiments.

structs expressed to varying levels, likely reflecting differences in their intrinsic stability (Fig. 1*C*). We found that only the full IDOL protein was capable of degrading the LDLR. Of note, in these cells we detect the LDLR as two bands, an endoplasmic reticulum precursor form and a lower mobility, fully glycosylated mature form that represents the form most susceptible to IDOL-mediated degradation. Importantly, the inability of the truncated proteins to degrade the LDLR is likely not a result of their decreased abundance. Titrating the level of full-length IDOL to a level comparable with that of the truncated forms still resulted in potent degradation of the LDLR (Fig. 1*D*). Collectively, these results indicate that degradation of the LDLR by IDOL is dependent on both protein domains and prompted us to study their specific activities.

The sequence of the IDOL RING is similar to that of other prototypical RING-containing E3 ubiquitin ligases (Fig. 2*A*)

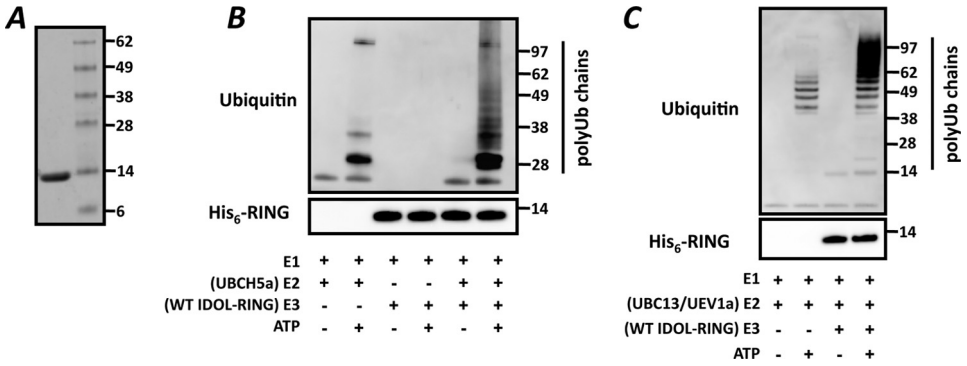

FIGURE 3. **IDOL promotes ubiquitination *in vitro*.** *A,* bacterially produced wild type His_6-IDOL RING was purified and 1 μg loaded on SDS-polyacrylamide gel. Grayscale image of Coomassie Brilliant Blue-stained gel is shown. *B* and *C, in vitro* ubiquitination assays were done with recombinant wild type RING proteins in combination with the E2-ubiquitin ligase UBCH5a (*B*) or UBC13/UEV1a (*C*). Subsequently, the reactions were analyzed by immunoblotting as indicated. Blots are representative of at least two independent experiments.

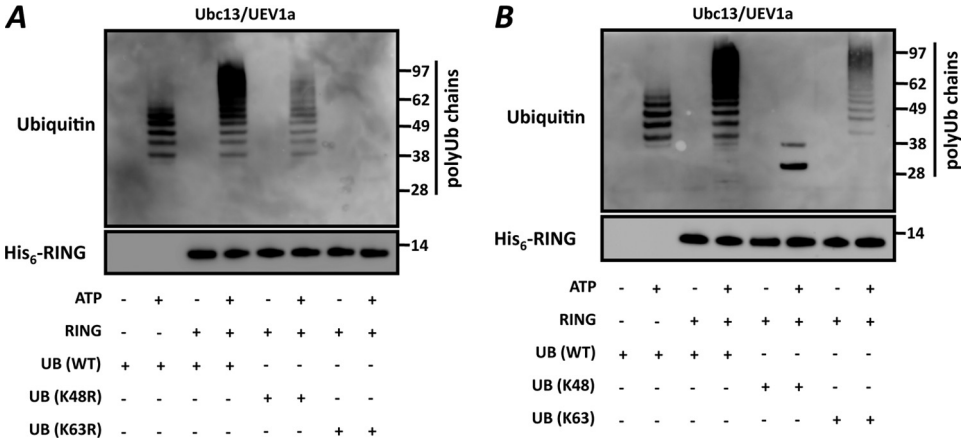

FIGURE 4. **IDOL promotes formation of Lys-63-specific linked ubiquitin chains *in vitro*.** *A* and *B, in vitro* ubiquitination assays were done with recombinant wild type RING protein and the E2-ubiquitin (*Ub*) ligase complex UBC13-UEV1a. The different ubiquitin mutants that were used in these assays are indicated. Subsequently, the reactions were analyzed by immunoblotting. Blots are representative of at least two independent experiments.

(16). A central function of the RING domains is to form a docking surface for the cognate E2-ubiquitin ligase (E2). This interaction depends on specific RING residues that make contact with the E2. We therefore generated RING mutations based on the reported structures of the E2-E3 ubiquitin ligase pairs UbcH7-Cbl (17) and UbcH13-K3 (18) and tested their functional consequence. None of the mutations we generated, including V389A and V420A that correspond to the detrimental Ile-383 and Phe-418 in c-Cbl (17), resulted in marked changes in degradation of the LDLR (Fig. 2*B*) or VLDLR (Fig. 2*C*). Rather, mutation of Leu-415, Pro-419, Val-420, and Arg-422 led to a varied increase in IDOL protein stability and abundance (Fig. 2, *B* and *C* and data not shown). This is akin to our previously reported mutation in one of the RING-forming cysteines (C387A) (11). However, in contrast to the RING-disrupting C387A mutation that stabilizes IDOL yet prevents it from degrading the LDLR, these newly identified residues stabilize IDOL and leave LDLR degradation unaffected. To further mechanistically substantiate the function of the IDOL RING domains, we generated and purified recombinant wild type IDOL RING protein (Fig. 3*A*). We initially tested the ability of the RING protein to promote ubiquitination *in vitro* with UBCH5a, a model E2. In line with our cellular-based results, recombinant IDOL RING promoted polyubiquitin chain formation in an E2- and ATP-dependent manner (Fig. 3*B*). The specific attachment of polyubiquitin chains linked through lysine 63 (Lys-63) of ubiquitin to membrane receptors is often associated with their lysosomal degradation (33). Since we recently reported that both the LDLR and VLDLR are targeted for lysosomal degradation by IDOL (11, 13), we tested whether the IDOL RING can also facilitate Lys-63 linkage formation in cooperation with the E2-ligase complex UBC13-UEV1a. This E2 has been previously shown to have basal Lys-63-specific ubiquitin linkage activity that is strongly stimulated in the presence of a compatible RING partner (19, 20). We observed that IDOL also strongly enhanced Lys-63-specific polyubiquitin chain formation in a RING- and ATP-dependent manner (Fig. 3*C*). In agreement with the established specificity of this E2 complex, we found that a mutant ubiquitin in which lysine 63 is replaced by an arginine (K63R) completely abolished UBC13/UEV1a-mediated ubiquitin chain formation independently of the RING domain (19, 20) (Fig. 4*A*). When we used a mutant ubiquitin containing only a single lysine at the 63 position, the RING domain could potently stimulate formation of Lys-63 polyubiquitin chains (Fig. 4*B*).

How IDOL-dependent ubiquitination leads to lysosomal degradation of the LDLR has not been resolved yet. We hypothesized that this may depend on the nature of the ubiquitin linkage formed by IDOL on the LDLR. In agreement with the *in vitro* ubiquitination assays, we determined that transfection of

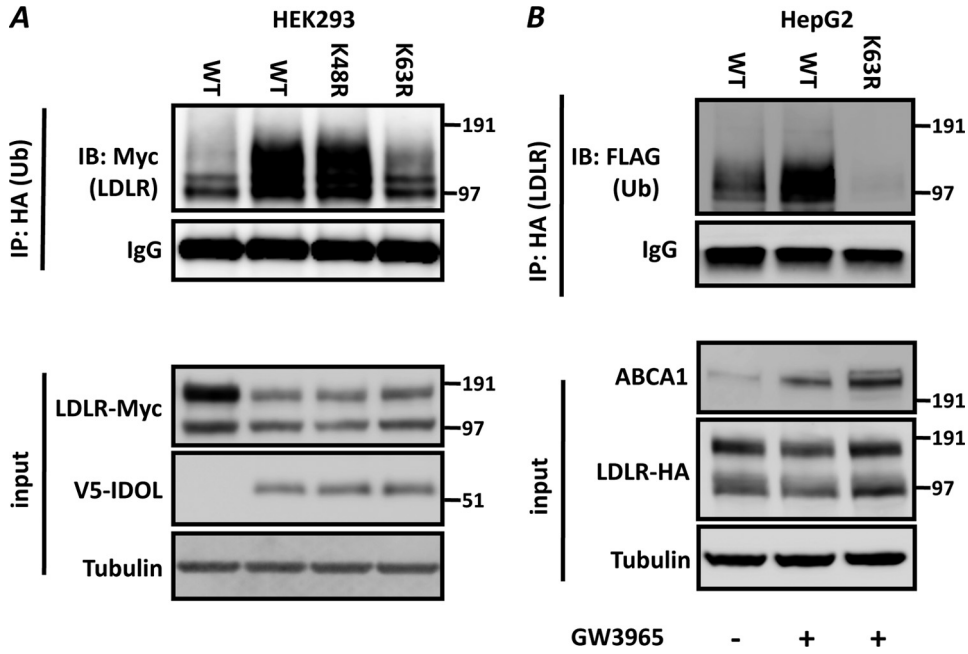

FIGURE 5. **IDOL promotes Lys-63-specific ubiquitination of the LDLR in cells.** *A,* HEK 293T cells were transfected with the indicated LDLR-Myc (200 ng), wild type V5-IDOL (800 ng), and HA-ubiquitin (*Ub*) (250 ng) expression plasmids. Samples were analyzed by immunoblotting (*IB*) as indicated. *B,* HepG2 cells were transfected with the indicated LDLR-HA (500 ng) and FLAG-ubiquitin (500 ng) expression plasmids as indicated. Subsequently, cells were treated for 6 h with 1 μM GW3965 to induce expression of *IDOL* before addition of the lysosomotropic agent bafilomycin A (100 nM) for an additional 4 h. Blots are representative of two independent experiments. *IP*, immunoprecipitation.

IDOL together with different ubiquitin mutants promotes Lys-63-specific ubiquitination of the LDLR in cells (Fig. 5*A*). As IDOL is subject to transcriptional regulation by LXR, we now asked whether activating LXR with a synthetic agonist ligand leads to a similar outcome. As we reported previously (11), treatment of HepG2 cells with GW3965, a synthetic LXR agonist, increased expression of the canonical LXR target gene *ABCA1* ($196 \pm 19\%$, $n = 5$, $p < 0.01$) and of *IDOL* ($702 \pm 125\%$, $n = 5$, $p < 0.01$). This treatment also increased endogenous ABCA1 in HepG2 cells further confirming the activation of LXR (Fig. 5*B*). To accumulate ubiquitinated LDLR, we used the lysosomotropic agent bafilomycin A. We have previously shown that inhibiting lysosomal degradation attenuates LXR- and IDOL-dependent degradation of the LDLR (11, 13). This likely explains the lack of a substantial decrease in abundance of LDLR under these experimental conditions. Nevertheless, concomitant to activation of the LXR-IDOL axis, we observed appearance of Lys-63-specific ubiquitinated LDLR (Fig. 5*B*).

Having established the role of the RING domain in receptor ubiquitination, we now turned our focus to the N-terminal FERM domain. The FERM domain forms the signature for members of the ERM family of proteins and is known to mediate the interaction between membranes and membrane proteins (21). We therefore predicted that this region in IDOL holds the interaction site with the LDLR and tested this using co-immunoprecipitation. In these experiments, we could not use full-length IDOL as it would degrade the LDLR and catalyze its own auto-ubiquitination and degradation (11). Instead, we used an IDOL FERM construct (IDOL residues 1–344) and found that it interacted with two LDLR family members and degradation targets of IDOL, the LDLR and VLDLR (Fig. 6, *A* and *B*). We used a similar approach to also address the cellular site of the IDOL-LDLR interaction by co-transfecting HepG2 cells with expression constructs for LDLR-GFP, FERM-DsRed2, or a mixture of both. When expressed separately in HepG2 cells, the LDLR localized predominantly to the plasma membrane and the FERM domain to intracellular vesicles (Fig. 7, *A* and *B*). Remarkably, co-expression of both constructs shifted the localization of the FERM domain toward the plasma membrane where it largely co-localized with the LDLR (Fig. 7, *C–H*).

The interaction interface between several FERM domains and their cognate membrane-protein substrates has been resolved by atomic resolution (22, 23). We therefore modeled the IDOL FERM domain on the solved structure of the FERM domain of protein 4.1 (PDB 1gg3) (14). Bioinformatic analysis revealed the presence of a putative phosphotyrosine-binding domain (PTB) also seen in the modeled structure. The PTB domains of the adaptor proteins ARH and DAB1 form an important structural determinant for binding LDLR family members (6, 15). Therefore, we overlaid the model of the IDOL PTB domain with the crystal structure of DAB1 bound to an APOER2 peptide (Fig. 8, *A* and *B*). Remarkably, the sequence of the predicted α-helix within the PTB domain of IDOL is highly evolutionarily conserved (Fig. 8*C*). In fact, it is even conserved in the distant fly homolog, Dnr1, which we have recently shown to also promote LDLR degradation (13). Accordingly, deleting this helix (IDOL residues 265–272, *underlined* in Fig. 8*C*) results in an IDOL protein that is unable to degrade the LDLR (data not shown). Within this helix, Tyr-265 and His-272 are predicted from our model to contribute to the IDOL-LDLR interaction. Mutating these residues strongly attenuated degradation of the LDLR by IDOL (Fig. 8*D*), whereas mutation of the

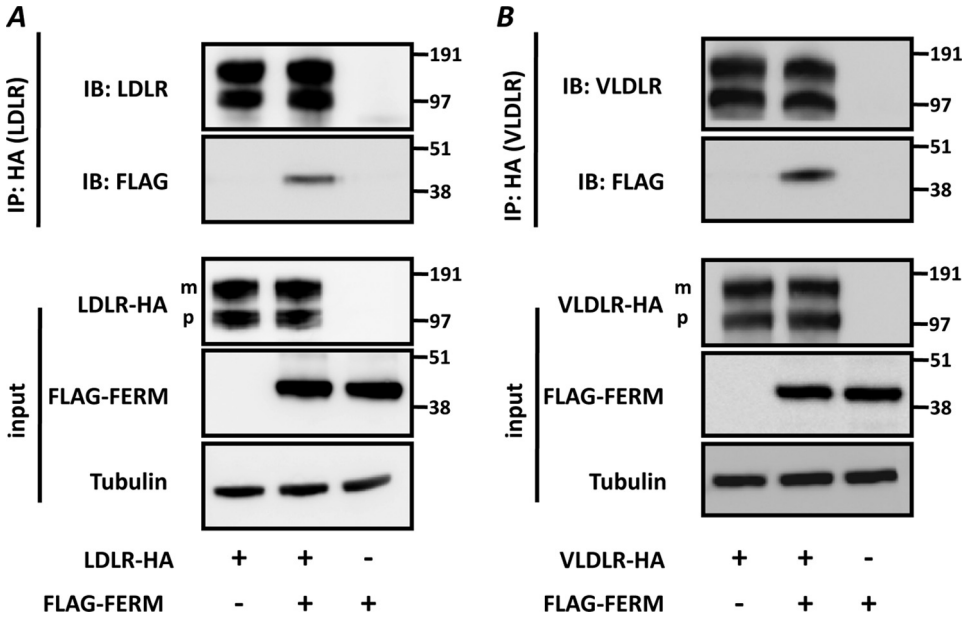

FIGURE 6. **IDOL FERM domain interacts with LDLR and VLDLR.** *A* and *B,* HEK293T cells were transfected with LDLR-HA (500 ng) or VLDLR-HA (500 ng) and FLAG-FERM (500 ng) expression plasmids. Total cell lysates and immunoprecipitated (*IP*) LDLR (*A*) and VLDLR (*B*) were analyzed by immunoblotting (*IB*) as indicated. The precursor (*p*) and mature (*m*) forms of the LDLR and VLDLR are indicated. The FLAG-FERM contains IDOL residues 1–344. Blots are representative of at least two independent experiments.

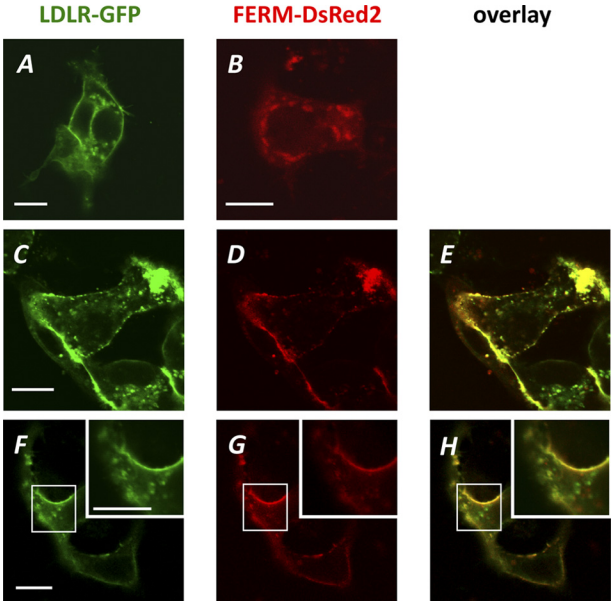

FIGURE 7. **LDLR-GFP and FERM-DsRed2 co-localize in cells.** HepG2 cells were transfected with LDLR-GFP (500 ng) (*A*), FERM-DsRed2 (500 ng) (*B*), or a mixture of both at a ratio of 1:1 (*C–H*). Representative live cells were imaged for LDLR-GFP (*A, C,* and *F*) and DsRed2 (*B, D,* and *G*) 48 h later. An overlay of images *C* and *D* and *F* and *G* was used to assess co-localization as shown in *E* and *H*, respectively. *Inset,* higher magnification image of *boxed area*. *Scale bar,* 5 μm.

adjacent Ile-268 and Tyr-269 had no effect (Fig. 8*D* and data not shown). The cellular localization of the Y265A and H272A mutants was indistinguishable from that of WT IDOL as assessed by indirect immunofluorescence, ruling this out as an explanation for their decreased ability to promote degradation of the LDLR (data not shown). Notably, at higher IDOL/LDLR ratios, the Y265A and H272A mutants were able to degrade the LDLR (Fig. 9, *A* and *B*), albeit to a lower extent than an equivalent level of wild type IDOL. Therefore, the most parsimonious explanation for the reduced activity of the PTB mutants is that mutation of Tyr-265 and His-272 decreased the affinity of IDOL for the LDLR.

Our model also allowed us to reciprocally address the region within the LDLR important for interaction with IDOL. We have previously reported that the intracellular tail of the LDLR is both required and sufficient for IDOL-dependent degradation (11, 13). Our model predicts that the residues immediately preceding the NPVY endocytosis motif in the LDLR interact with IDOL. In fact, this region is highly conserved in the different receptors marked by IDOL for degradation (Fig. 10*A*). As we have previously reported, deleting the complete intracellular domain of the LDLR (residues 811–860, $LDLR_{\Delta IC}$) decreases abundance of the transfected receptor and produces a receptor resistant to IDOL (Fig. 10*B*). As a first step to establish the LDLR residues that bind to IDOL, we deleted residues 817–824 in the LDLR (LDLR(Δ817–824)) that partially overlap with those contributing to binding of the APOER2 peptide to DAB1. Deleting these residues in the LDLR resulted in a receptor insensitive to IDOL-mediated degradation (Fig. 10*B*). Notably, a closely related LDLR family member, Lrp1b, is not degraded by IDOL (13). We therefore hypothesized that sequence divergence between LDLR family members targeted by IDOL and Lrp1b may determine specific recognition by IDOL (Fig. 10*A*). To test this hypothesis, we introduced corresponding Lrp1b residues into the LDLR and identified the highly conserved Phe-823 and Asp-824 as important specificity determinants for interaction with IDOL (Fig. 10*C*). Mutating these residues resulted in an LDLR substantially less sensitive to IDOL-mediated degradation.

DISCUSSION

We have recently identified the E3 ubiquitin ligase IDOL as a direct transcriptional target of LXR and a novel post-transla-

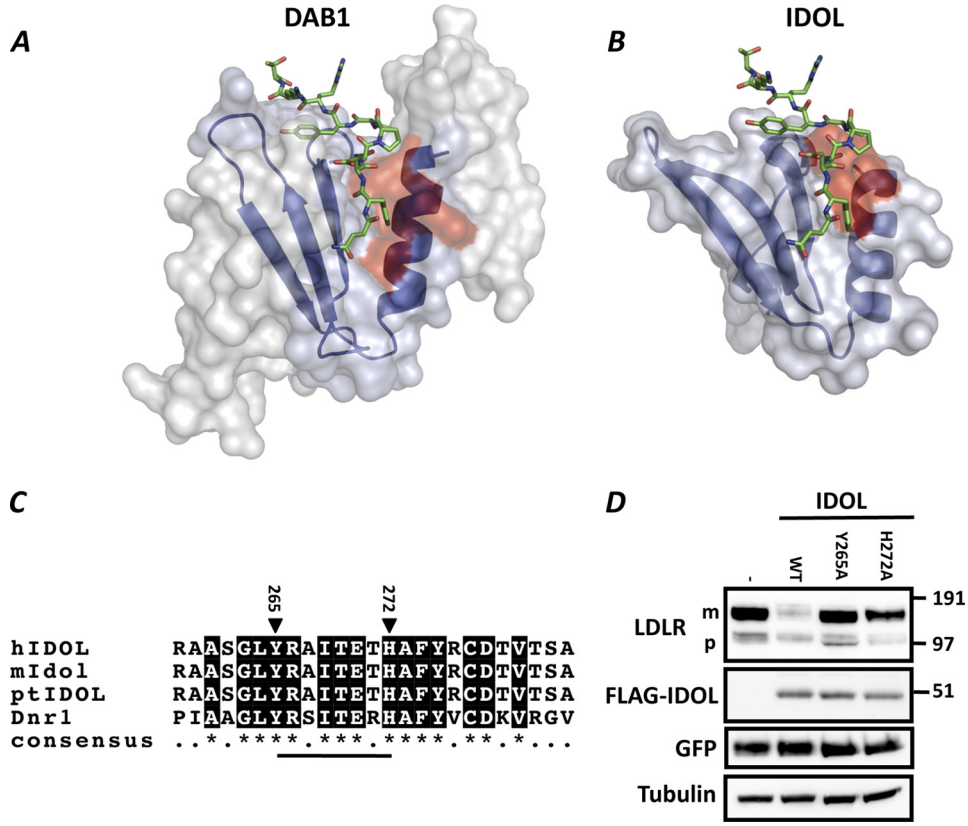

FIGURE 8. **Homology modeling identifies IDOL residues involved in LDLR binding.** *A* and *B,* DAB1 (*A*) and homology modeled IDOL (*B*) PTB domains are depicted as a schematic in *blue*. The DAB1 structure bound with APOER2 peptide was adapted from Stolt *et al.* (15), PDB accession 1NTV. The APOER2 peptide is shown for both complexes. Residues in DAB1 proposed to interact with the ApoER2 peptide and corresponding residues in IDOL are depicted in *red*. *C,* sequence alignment of the α-helical segment in the IDOL PTB domain. *Numbering* corresponds to residue number in hIDOL. *Closed triangles* indicate residues that were mutated in this study. *D,* HEK293T cells were co-transfected with LDLR (500 ng), the indicated IDOL mutants (100 ng), and GFP (50 ng) expression plasmids. Total cell lysates were analyzed by immunoblotting as shown. The precursor (*p*) and mature (*m*) forms of the LDLR are indicated. Immunoblot is representative of at least two independent experiments.

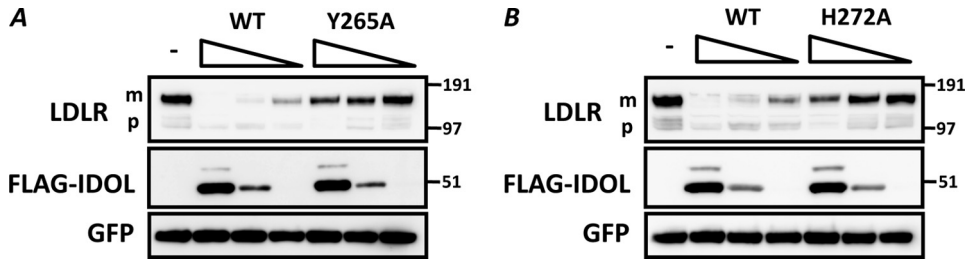

FIGURE 9. Decreased degradation of the LDLR by IDOL Y265A and H272A mutants (*A*). *A* and *B,* HEK 293T cells were co-transfected with LDLR (500 ng), the indicated wild type or mutant FLAG-tagged IDOL (450, 150, and 50 ng), and GFP (50 ng) expression plasmids. An equal amount of total DNA was maintained in the transfection reactions. Total cell lysates were analyzed by immunoblotting as indicated. The precursor (*p*) and mature (*m*) forms of the LDLR are indicated. Blots are representative of at least two independent experiments.

tional regulator of a subset of LDLR family receptors (11, 13). IDOL is a unique ERM family member in that it contains a RING unit in addition to the signature FERM domain (10, 21). Independently, neither of these functionally defined protein domains is able to enhance LDLR degradation. This prompted us to dissect the roles of each domain independently as a means to gain insight into the mechanism governing LDLR degradation by IDOL.

RING-containing E3 ubiquitin ligases constitute one of the largest mammalian protein families (16). Overall, the IDOL RING domain is homologous to that of other members of this protein family and, intriguingly, contains three extra cysteine residues in addition to the seven forming the conserved RING structure. We have previously demonstrated that IDOL promotes appearance of ubiquitinated LDLR in cells (11). The ability of the IDOL RING domain to stimulate polyubiquitin chain formation *in vitro* formally establishes IDOL as a *bona fide* E3 ubiquitin ligase. Unexpectedly, a set of RING mutants (L415A, V420A, and R422A) that we generated based on reported E2-E3 co-structures did not abrogate degradation of the LDLR by IDOL. Rather, these increased IDOL protein stability. This finding raises the possibility that the ubiquitination of the LDLR and auto-ubiquitination of IDOL are dissociated and independent of each other. In fact, this may account for our reported observation that although IDOL degradation is a proteosomal event, IDOL-mediated degradation of the LDLR and

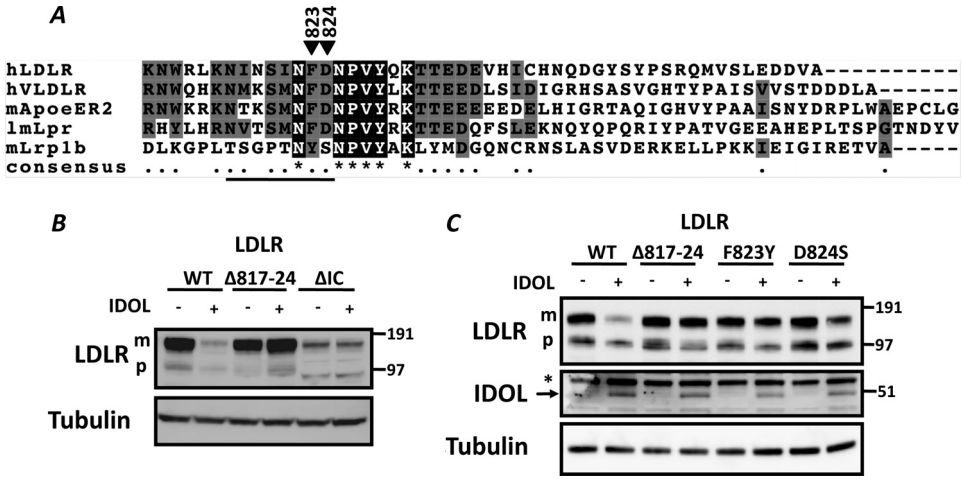

FIGURE 10. **IDOL-mediated degradation of the LDLR requires conserved residues in the intracellular tail of the receptor.** *A,* intracellular domains of hLDLR, hVLDLR, mApoer2, lmLpr, and mLrp1b are shown. *Triangles* depict the highly conserved residues whose mutation attenuates LDLR degradation by IDOL. *Numbering* corresponds to the hLDLR. The *solid line* depicts LDLR residues 817–24 that are deleted in Δ817–824. *B* and *C,* HEK 293T cells were co-transfected with the indicated LDLR mutants (900 ng) and IDOL (100 ng) expression plasmids. Total cell lysates were analyzed by immunoblotting as indicated. Note: → indicates IDOL; * indicates a nonspecific band. *Δ817–824* and *ΔIC,* LDLR lacking residues 817–824 or the complete intracellular tail (LDLR residues 811–860), respectively. The precursor (*p*) and mature (*m*) forms of the LDLR are indicated. Immunoblots are representative of at least two independent experiments.

VLDLR is lysosomal (11, 13). At present, we cannot formally rule out that the interaction of IDOL with a single E2 ligase mediates both outcomes. However, we find it more plausible that differential E2 ligase recruitment to IDOL determines the outcome of the ubiquitination reaction as most E2 ligases have a preference for forming specific polyubiquitin chain linkages (24, 25). The ability of E3 ligases to interact with multiple E2 partners is supported by recent global E2-E3 interaction screens (26, 27). Furthermore, it is now clear that specific E2-E3 interactions can control the nature of the ubiquitin linkage that is formed, as was shown for the BRCA1 RING (28). Also, the recruitment of multiple E2 ligases into a single degradation complex is not unprecedented. The APC complex, for instance, concomitantly recruits the E2 ligases UbcH10 and Ube2S, and both are necessary for Lys-11-linked polyubiquitination of mitotic targets (29). We therefore speculate that interaction with one E2 partner would promote IDOL polyubiquitination and proteosomal degradation, whereas interaction with an alternative E2 promotes Lys-63 ubiquitination of the LDLR and its subsequent lysosomal destruction. The identities of the cognate IDOL-interacting E2 ligases remain to be determined. One possibility is that E2 ligases are recruited to IDOL sequentially. An alternative scenario, supported by our preliminary results indicating that IDOL forms dimers, is that these oligomeric manifolds may act as a scaffold for differential E2 recruitment.

The second functional domain present in IDOL is the N-terminal FERM. The FERM domain defines a protein family known to interact with membrane proteins that is implicated in numerous physiological processes (21). Accordingly, we demonstrate an interaction between the IDOL FERM domain and the target receptors LDLR and VLDLR. In the model hepatocyte cell line HepG2, the FERM-DsRed2 and LDLR-GFP signal largely overlapped. The co-localization was largely confined to the plasma membrane and vesicles juxtaposed with it. This was in stark contrast to the intracellular and vesicular localization of the FERM protein in the absence of the LDLR. In preliminary experiments, we ruled out the possibility that activation of LXR in HepG2 cells is able to redistribute the FERM-DsRed2 protein toward the plasma membrane. As such, the straightforward interpretation of this result is that IDOL interacts with the LDLR at or near the plasma membrane, akin to other adaptor proteins like DAB1 and ARH involved in receptor endocytosis (6, 30, 31). This localization points toward the recycling LDLR pool as the target for IDOL-mediated degradation. This strategy seems appropriate to oppose the transcriptional regulation of the *LDLR* by SREBP when the cellular sterol burden increases (5). By removing circulating LDLR, activation of the LXR-IDOL axis rapidly diminishes receptor abundance, shuts off LDL uptake, and circumvents the long half-life of the LDLR (32).

We have not determined the precise endocytic compartment in which ubiquitination of the LDLR by IDOL takes place. However, it is important to emphasize that ubiquitination of the LDLR by IDOL is not a prerequisite step for receptor endocytosis. Knocking down endogenous IDOL expression increases abundance of the LDLR and LDL uptake into cells indicating that receptor endocytosis remains intact (11). We determined that IDOL, or activation of the LXR transcriptional program, promotes Lys-63-specific ubiquitination of the LDLR. There is accumulating evidence that within the endocytic system, Lys-63 ubiquitin linkage is specifically involved in receptor sorting and trafficking (33). We therefore propose that ubiquitination of the LDLR by IDOL acts as a sorting signal that directs the receptor toward the lysosomal degradation pathway.

Having established that the FERM region mediates the interaction between IDOL and the LDLR allowed us to perform initial characterization of the interaction interface. Analysis of the homology model of the IDOL PTB and the DAB1-APOER2 crystal structure (15) identified a structurally conserved α-helix that forms part of a receptor-binding pocket. Several residues within this helix contribute to APOER2 binding to DAB1 and mutation of the equivalent residues in IDOL identified Tyr-265

and His-272 as important determinants of LDLR degradation. Their mutation attenuated LDLR degradation by IDOL, most likely by reducing the affinity of IDOL to the LDLR. In a reciprocal manner, we could also demonstrate that the sequence preceding the NPVY endocytosis motif in the LDLR is critical for IDOL-dependent degradation. Consistent with the DAB1-APOER2 structure, it was sufficient to mutate the two residues immediately preceding this motif to strongly attenuate degradation of the LDLR by IDOL. This is in good agreement with Beffert *et al.* (34) who demonstrated that replacing three residues upstream of the NPVY motif is sufficient to prevent DAB1 from binding APOER2 both *in vitro* and *in vivo*. Overall, our results support the presence of a well defined binding interface between IDOL and the LDLR with residues from both proteins contributing to the interaction network.

In conclusion, we provide a detailed mechanistic analysis of the functional domains in IDOL that contribute to LDLR recognition and degradation. We propose that IDOL forms a unique interaction interface with the LDLR and its E2 counterpart. Recent genome-wide association studies identify IDOL as a novel modulator of LDL in humans, thus implicating IDOL as a potential therapeutic target (35–37). Our current results support the investigation of the development of IDOL interaction inhibitors as a novel therapeutic approach to treat dyslipidemia and cardiovascular disease.

Acknowledgments—We thank Ben Distel, Hans Aerts, Carlie de Vries, Arthur Verhoeven, Peter Tontonoz, John Schwabe, Ben Goult, and Irith Koster for their comments and suggestions.

REFERENCES

1. Hobbs, H. H., Russell, D. W., Brown, M. S., and Goldstein, J. L. (1990) *Annu. Rev. Genet.* **24,** 133–170
2. Russell, D. W., Schneider, W. J., Yamamoto, T., Luskey, K. L., Brown, M. S., and Goldstein, J. L. (1984) *Cell* **37,** 577–585
3. Brown, M. S., and Goldstein, J. L. (1986) *Science* **232,** 34–47
4. Tolleshaug, H., Hobgood, K. K., Brown, M. S., and Goldstein, J. L. (1983) *Cell* **32,** 941–951
5. Goldstein, J. L., DeBose-Boyd, R. A., and Brown, M. S. (2006) *Cell* **124,** 35–46
6. Garcia, C. K., Wilund, K., Arca, M., Zuliani, G., Fellin, R., Maioli, M., Calandra, S., Bertolini, S., Cossu, F., Grishin, N., Barnes, R., Cohen, J. C., and Hobbs, H. H. (2001) *Science* **292,** 1394–1398
7. Cohen, J., Pertsemlidis, A., Kotowski, I. K., Graham, R., Garcia, C. K., and Hobbs, H. H. (2005) *Nat. Genet.* **37,** 161–165
8. Park, S. W., Moon, Y. A., and Horton, J. D. (2004) *J. Biol. Chem.* **279,** 50630–50638
9. Abifadel, M., Varret, M., Rabès, J. P., Allard, D., Ouguerram, K., Devillers, M., Cruaud, C., Benjannet, S., Wickham, L., Erlich, D., Derré, A., Villéger, L., Farnier, M., Beucler, I., Bruckert, E., Chambaz, J., Chanu, B., Lecerf, J. M., Luc, G., Moulin, P., Weissenbach, J., Prat, A., Krempf, M., Junien, C., Seidah, N. G., and Boileau, C. (2003) *Nat. Genet.* **34,** 154–156
10. Olsson, P. A., Korhonen, L., Mercer, E. A., and Lindholm, D. (1999) *J. Biol. Chem.* **274,** 36288–36292
11. Zelcer, N., Hong, C., Boyadjian, R., and Tontonoz, P. (2009) *Science* **325,** 100–104
12. Zelcer, N., and Tontonoz, P. (2006) *J. Clin. Invest.* **116,** 607–614
13. Hong, C., Duit, S., Jalonen, P., Out, R., Scheer, L., Sorrentino, V., Boyadjian, R., Rodenburg, K. W., Foley, E., Korhonen, L., Lindholm, D., Nimpf, J., van Berkel, T. J., Tontonoz, P., and Zelcer, N. (2010) *J. Biol. Chem.* **285,** 19720–19726
14. Han, B. G., Nunomura, W., Takakuwa, Y., Mohandas, N., and Jap, B. K. (2000) *Nat. Struct. Biol.* **7,** 871–875
15. Stolt, P. C., Jeon, H., Song, H. K., Herz, J., Eck, M. J., and Blacklow, S. C. (2003) *Structure* **11,** 569–579
16. Deshaies, R. J., and Joazeiro, C. A. (2009) *Annu. Rev. Biochem.* **78,** 399–434
17. Zheng, N., Wang, P., Jeffrey, P. D., and Pavletich, N. P. (2000) *Cell* **102,** 533–539
18. Dodd, R. B., Allen, M. D., Brown, S. E., Sanderson, C. M., Duncan, L. M., Lehner, P. J., Bycroft, M., and Read, R. J. (2004) *J. Biol. Chem.* **279,** 53840–53847
19. Deng, L., Wang, C., Spencer, E., Yang, L., Braun, A., You, J., Slaughter, C., Pickart, C., and Chen, Z. J. (2000) *Cell* **103,** 351–361
20. Nakada, S., Tai, I., Panier, S., Al-Hakim, A., Iemura, S., Juang, Y. C., O'Donnell, L., Kumakubo, A., Munro, M., Sicheri, F., Gingras, A. C., Natsume, T., Suda, T., and Durocher, D. (2010) *Nature* **466,** 941–946
21. Bretscher, A., Edwards, K., and Fehon, R. G. (2002) *Nat. Rev. Mol. Cell Biol.* **3,** 586–599
22. Goult, B. T., Bate, N., Anthis, N. J., Wegener, K. L., Gingras, A. R., Patel, B., Barsukov, I. L., Campbell, I. D., Roberts, G. C., and Critchley, D. R. (2009) *J. Biol. Chem.* **284,** 15097–15106
23. Hamada, K., Shimizu, T., Yonemura, S., Tsukita, S., Tsukita, S., and Hakoshima, T. (2003) *EMBO J.* **22,** 502–514
24. Ye, Y., and Rape, M. (2009) *Nat. Rev. Mol. Cell Biol.* **10,** 755–764
25. Rodrigo-Brenni, M. C., Foster, S. A., and Morgan, D. O. (2010) *Mol. Cell* **39,** 548–559
26. Markson, G., Kiel, C., Hyde, R., Brown, S., Charalabous, P., Bremm, A., Semple, J., Woodsmith, J., Duley, S., Salehi-Ashtiani, K., Vidal, M., Komander, D., Serrano, L., Lehner, P., and Sanderson, C. M. (2009) *Genome Res.* **19,** 1905–1911
27. van Wijk, S. J., de Vries, S. J., Kemmeren, P., Huang, A., Boelens, R., Bonvin, A. M., and Timmers, H. T. (2009) *Mol. Syst. Biol.* **5,** 295
28. Christensen, D. E., Brzovic, P. S., and Klevit, R. E. (2007) *Nat. Struct. Mol. Biol.* **14,** 941–948
29. Garnett, M. J., Mansfeld, J., Godwin, C., Matsusaka, T., Wu, J., Russell, P., Pines, J., and Venkitaraman, A. R. (2009) *Nat. Cell Biol.* **11,** 1363–1369
30. Gotthardt, M., Trommsdorff, M., Nevitt, M. F., Shelton, J., Richardson, J. A., Stockinger, W., Nimpf, J., and Herz, J. (2000) *J. Biol. Chem.* **275,** 25616–25624
31. Michaely, P., Li, W. P., Anderson, R. G., Cohen, J. C., and Hobbs, H. H. (2004) *J. Biol. Chem.* **279,** 34023–34031
32. Basu, S. K., Goldstein, J. L., Anderson, R. G., and Brown, M. S. (1981) *Cell* **24,** 493–502
33. Mukhopadhyay, D., and Riezman, H. (2007) *Science* **315,** 201–205
34. Beffert, U., Durudas, A., Weeber, E. J., Stolt, P. C., Giehl, K. M., Sweatt, J. D., Hammer, R. E., and Herz, J. (2006) *J. Neurosci.* **26,** 2041–2052
35. Waterworth, D. M., Ricketts, S. L., Song, K., Chen, L., Zhao, J. H., Ripatti, S., Aulchenko, Y. S., Zhang, W., Yuan, X., Lim, N., Luan, J., Ashford, S., Wheeler, E., Young, E. H., Hadley, D., Thompson, J. R., Braund, P. S., Johnson, T., Struchalin, M., Surakka, I., Luben, R., Khaw, K. T., Rodwell, S. A., Loos, R. J., Boekholdt, S. M., Inouye, M., Deloukas, P., Elliott, P., Schlessinger, D., Sanna, S., Scuteri, A., Jackson, A., Mohlke, K. L., Tuomilehto, J., Roberts, R., Stewart, A., Kesäniemi, Y. A., Mahley, R. W., Grundy, S. M., McArdle, W., Cardon, L., Waeber, G., Vollenweider, P., Chambers, J. C., Boehnke, M., Abecasis, G. R., Salomaa, V., Järvelin, M. R., Ruokonen, A., Barroso, I., Epstein, S. E., Hakonarson, H. H., Rader, D. J., Reilly, M. P., Witteman, J. C., Hall, A. S., Samani, N. J., Strachan, D. P., Barter, P., van Duijn, C. M., Kooner, J. S., Peltonen, L., Wareham, N. J., McPherson, R., Mooser, V., and Sandhu, M. S. (2010) *Arterioscler. Thromb. Vasc. Biol.* **30,** 2264–2276
36. Teslovich, T. M., Musunuru, K., Smith, A. V., Edmondson, A. C., Stylianou, I. M., Koseki, M., Pirruccello, J. P., Ripatti, S., Chasman, D. I., Willer, C. J., Johansen, C. T., Fouchier, S. W., Isaacs, A., Peloso, G. M., Barbalic, M., Ricketts, S. L., Bis, J. C., Aulchenko, Y. S., Thorleifsson, G., Feitosa, M. F., Chambers, J., Orho-Melander, M., Melander, O., Johnson, T., Li, X., Guo, X., Li, M., Shin Cho, Y., Jin Go, M., Jin Kim, Y., Lee, J. Y., Park, T., Kim, K., Sim, X., Twee-Hee Ong, R., Croteau-Chonka, D. C., Lange, L. A., Smith, J. D., Song, K., Hua Zhao, J., Yuan, X., Luan, J., Lamina, C., Ziegler, A., Zhang, W., Zee, R. Y., Wright, A. F., Witteman, J. C., Wilson, J. F.,

Willemsen, G., Wichmann, H. E., Whitfield, J. B., Waterworth, D. M., Wareham, N. J., Waeber, G., Vollenweider, P., Voight, B. F., Vitart, V., Uitterlinden, A. G., Uda, M., Tuomilehto, J., Thompson, J. R., Tanaka, T., Surakka, I., Stringham, H. M., Spector, T. D., Soranzo, N., Smit, J. H., Sinisalo, J., Silander, K., Sijbrands, E. J., Scuteri, A., Scott, J., Schlessinger, D., Sanna, S., Salomaa, V., Saharinen, J., Sabatti, C., Ruokonen, A., Rudan, I., Rose, L. M., Roberts, R., Rieder, M., Psaty, B. M., Pramstaller, P. P., Pichler, I., Perola, M., Penninx, B. W., Pedersen, N. L., Pattaro, C., Parker, A. N., Pare, G., Oostra, B. A., O'Donnell, C. J., Nieminen, M. S., Nickerson, D. A., Montgomery, G. W., Meitinger, T., McPherson, R., McCarthy, M. I., McArdle, W., Masson, D., Martin, N. G., Marroni, F., Mangino, M., Magnusson, P. K., Lucas, G., Luben, R., Loos, R. J., Lokki, M. L., Lettre, G., Langenberg, C., Launer, L. J., Lakatta, E. G., Laaksonen, R., Kyvik, K. O., Kronenberg, F., König, I. R., Khaw, K. T., Kaprio, J., Kaplan, L. M., Johansson, A., Jarvelin, M. R., Janssens, A. C., Ingelsson, E., Igl, W., Kees Hovingh, G., Hottenga, J. J., Hofman, A., Hicks, A. A., Hengstenberg, C., Heid, I. M., Hayward, C., Havulinna, A. S., Hastie, N. D., Harris, T. B., Haritunians, T., Hall, A. S., Gyllensten, U., Guiducci, C., Groop, L. C., Gonzalez, E., Gieger, C., Freimer, N. B., Ferrucci, L., Erdmann, J., Elliott, P., Ejebe, K. G., Döring, A., Dominiczak, A. F., Demissie, S., Deloukas, P., de Geus, E. J., de Faire, U., Crawford, G., Collins, F. S., Chen, Y. D., Caulfield, M. J., Campbell, H., Burtt, N. P., Bonnycastle, L. L., Boomsma, D. I., Boekholdt, S. M., Bergman, R. N., Barroso, I., Bandinelli, S., Ballantyne, C. M., Assimes, T. L., Quertermous, T., Altshuler, D., Seielstad, M., Wong, T. Y., Tai, E. S., Feranil, A. B., Kuzawa, C. W., Adair, L. S., Taylor, H. A., Jr., Borecki, I. B., Gabriel, S. B., Wilson, J. G., Holm, H., Thorsteinsdottir, U., Gudnason, V., Krauss, R. M., Mohlke, K. L., Ordovas, J. M., Munroe, P. B., Kooner, J. S., Tall, A. R., Hegele, R. A., Kastelein, J. J., Schadt, E. E., Rotter, J. I., Boerwinkle, E., Strachan, D. P., Mooser, V., Stefansson, K., Reilly, M. P., Samani, N. J., Schunkert, H., Cupples, L. A., Sandhu, M. S., Ridker, P. M., Rader, D. J., van Duijn, C. M., Peltonen, L., Abecasis, G. R., Boehnke, M., and Kathiresan, S. (2010) *Nature* **466,** 707–713

37. Chasman, D. I., Paré, G., Mora, S., Hopewell, J. C., Peloso, G., Clarke, R., Cupples, L. A., Hamsten, A., Kathiresan, S., Mälarstig, A., Ordovas, J. M., Ripatti, S., Parker, A. N., Miletich, J. P., and Ridker, P. M. (2009) *PLoS Genet.* **5,** e1000730